Structural phase transition of alkane molecules in nanotube composites

Chenyu Wei*

NASA Ames Research Center, MS 229-1, Moffett Field, California 94035, USA

The structural phase transition and crystallization process of alkane molecules in carbon nanotube (CNT) composites are studied through molecular dynamics simulations. An isotropic-to-nematic transition with molecules aligned with embedded nanotubes is found. Further smectic transition of the alkane molecules is found with small radius armchaired CNT (5, 5) as a nucleation site, where molecules form lamellar layers along the nanotube axis and have two-dimensional structure ordering in planes perpendicular to the tube axis, in analogy to a crystalline polymer. While the translational diffusions are limited in the smectic phase, the molecules have rotation freedom along its long axis with small energy barriers $\sim 1-2k_B T$ ($T=300$ K) for decane molecules studied here. The molecule crystallization is found to strongly dependent on CNT chirality, where a lack of two-dimensional ordering of molecules around a similar radius zigzag CNT (10, 0) is due to diverse molecule assembly domains with tilted wrapping angles at the interface, controlled by the interactions with the substrate nanotube lattice. The influence of strength and nature of the interfacial interactions between molecules and nanotubes is also studied. The results in this study would be useful and important for the understanding of structural phases in hybrid polymer materials and for the designs of nanotube based high performance composites.

Carbon nanotubes (CNTs) have nanoscaled tubular structures, which sizes are comparable to polymer or biological molecules. Their composites or hybrid materials have unique structural, thermal, mechanical, and electronic properties, due to CNTs' high mechanical strength and thermal conductivity and strong structure and environment sensitive electronic properties.[1] CNTs have been investigated extensively as additive fibers in various multifunctional polymeric nanocomposites[2–7] and also as sensors for biopolymer molecules, such as DNAs.[8–11] Previous experiments[12–17] and theoretical studies[18] have shown that a CNT can induce strong structural or conformational changes in surrounding polymer molecules, and such changes can be chirality and radius dependent on the CNT lattice due to the interfacial interactions. Ordered assemblies and enhanced crystallization of polymer molecules around CNTs have also been shown in both experiment and simulation studies.[18–25] The molecule structure ordering is expected to strongly affect the properties of CNT based nanocomposites. For example, it is shown that high structural ordering contributes to high enhancements in modulus and strength of nanotube composites.[26–28] The understanding of structural phases in polymer nanotube composite not only has fundamental interests but also is important for the applications of nanocomposites or hybrid materials.

In this study, we investigate structural phase transitions of alkane molecules in CNT composites and their dependence on the atomic structure of nanotube lattice and the strength and nature of interfacial interactions, with molecular dynamics (MD) simulations.[29] Model alkane molecule is chosen due to its representative linear chained structure for polymer molecules. Molecule motions are dramatically slowed down with decreasing temperature in a polymeric material when the system goes to viscous or glassy states. A dynamic process involving structure changes in low temperature states is expected to be slow, and longer the polymer slower the process. To fasten simulations, we choose a short alkane mol-

ecule, decane ($C_{10}H_{22}$), as model polymer molecules in this study. The length effects will be discussed later.

AMBER force field[30] was used for the C-C interactions within a nanotube, which has been shown to give structural and elastic properties in good agreement with experiments and with more specific designed force fields,[28] such as the widely used Tersoff-Brenner potential.[31] A united atom force field was applied for alkane molecules, including bond stretching, angle bending, and dihedral angle rotation interactions. The interactions between polymer molecules and nanotubes are described through a truncated 12-6 type Lennard-Jones (LJ) potential. This kind of nonbonded van der Waals (vdw) potential is general in polymer CNT composites. The LJ potential is also used for intermolecule interactions within polymer matrix and for any two monomers separated beyond four bonds in each molecule. The details of the force field can be found elsewhere.[32] Composite systems in this study usually consist of 800 decane molecules and a continuous CNT about 210 Å long in a periodic simulation cell with size around $40 \times 40 \times 210$ Å^3 [as illustrated in the inset of Fig. 1(a)]. Each polymer molecule was prepared with a Monte Carlo simulation beforehand. The composite systems were prepared at a high temperature of 500 K, and cooled down to low T's (down to 100 K) at a rate of 100 ps/10 K. During the cooling process, the composites go through a liquid to glassy state. The details for sample preparation can be found in a previous study.[32] Berendsen *NPT* ensemble was used in most of the simulations ($P=1$ bar), except in the initial equilibration runs, where Evans *NVT* ensemble was used. The time step of 1 fs was used. The data present in this study are usually a statistical average over a 100 ps MD simulation time interval unless otherwise stated.

A system of decane molecules with an armchaired CNT (5, 5) is simulated for a temperature range from 500 to 100 K. The radial density function (RDF) $g(r)$ of the polymer molecules surrounding the nanotube is shown in
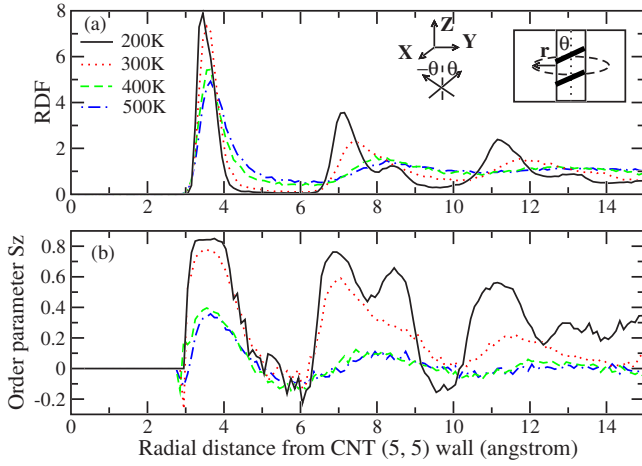
FIG. 1. (Color online) (a) The radial distribution function (RDF) for decane molecules in CNT (5, 5) composite. Inset: Schematic plot of an embedded CNT in a simulation unit cell and the definition of coordinates. The black strap represents a molecule around the CNT with a wrapping angle θ. The orientation vector of a subchain in a molecule is shown at symmetric angle $\pm\theta$ with the tube axis. (b) The orientation order parameter $S_z(r)$. Solid, dotted, dashed, and dot-dashed line are for $T=200$ K, 300 K, 400 K, and 500 K, respectively, in both (a) and (b).

Fig. 1(a), as a function of the radial distance r from the CNT wall.[33] Adsorption peaks at 3.5 ($\approx r^*$, the vdw equilibrium distance between C atoms on molecules and CNTs), 7.2, and 11.5 Å are shown. Similar oscillating features of $g(r)$ have been shown for molecules on nanotubes or on plat surfaces in previous studies.[18,34–36] With decreasing T, an enhancement in the magnitude of the molecule adsorption peaks is also seen in Fig. 1(a), which is attributed to the increased molecule packing at the interface. Different from the well separated adsorption peaks at high T's, a peak at $r=8.4$ Å adjoined to the second peak at $r=7.2$ Å appears at low T's (200 K), which is later shown due to the crystallization of the decane molecules around the nanotube.

The enhanced molecule structural ordering around the nanotube is further shown through an orientation ordering parameter $S_z(r)$, which measures the correlation between the orientation of a molecule backbone and CNT axis. $S_z(r)$ is defined as follows:[34,37]

$$S_z(r) = \frac{1}{2}\langle 3\cos^2\theta(r) - 1\rangle, \qquad (1)$$

where θ is the angle between the vector of a subchain with four segments on a same molecule and the nanotube axis with the center mass of the subchain at a radial distance r from the CNT wall, and $\langle\ \rangle$ represents the statistical average over all the molecules in the simulation. Parameter $S_z(r)$ measures the alignment of polymer molecules along the nanotube, with $S_z=1$, 0, and -0.5 for parallel, random, and perpendicular orientations, respectively, to the CNT axis. Shown in Fig. 1(b) is the function $S_z(r)$ at various temperatures. As it can be seen, the decane molecules begin to strongly align with the tube axis with decreasing T to reduce
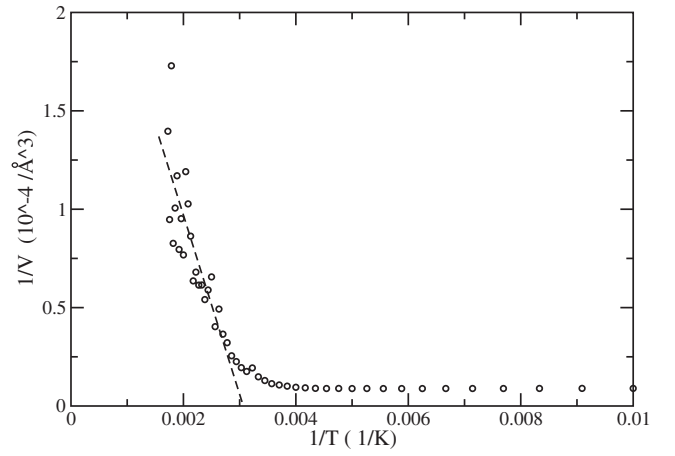

FIG. 2. The inverse of the correlation volume $1/V_\xi$ (Å^{-3}) as a function of $1/T$ (K^{-1}). The data calculated from $g(r)$ and $S_z(r)$ from Fig. 1 are represented in circles and the dashed line is the theoretical fitting according to Eq. (2) for $T>300$ K.

adsorption energies. At low T's (such as 300 or 200 K), the alignment is extended beyond the first adsorption layer. Such broad range alignment is due to a nematic phase transition in the system. According to Landau–de Gennes theory on isotropic-nematic transition,[37,38] a correlation volume is diverged at a transition temperature T_c as follows:

$$\frac{1}{V_\xi} = \alpha\left(\frac{1}{T} - \frac{1}{T_c}\right), \qquad (2)$$

where α is a constant and the correlation volume is defined as

$$V_\xi = 4\pi\int_0^\infty r^2 S_z(r)g(r)dr. \qquad (3)$$

Shown in Fig. 2 is the $1/V_\xi$ as a function of $1/T$, which is calculated from $g(r)$ and $S_z(r)$ as in Fig. 1. The drop of $1/V_\xi$ with the decreasing of T indicates a nematic phase transition. Fitting of $1/V_\xi$ at high T's according to Eq. (2) gives a transition temperature $T_c=325$ K by exploration to $1/V_\xi=0$ (dashed line in Fig. 2). For the decane CNT (5, 5) composite, the glass transition temperature T_g is estimated as 185 K from the density vs T function. The system is expected to be in a nematic phase at room temperature $T=300$ K, and the transition process should be fast enough in MD simulations as $T_g<300$ K $<T_c$.

To investigate the phase transition process, an additional simulation up to 7 ns was run for the system at $T=300$ K right after the cooling process. A nematic transition and a structural phase with two-dimensional ordering in planes perpendicular to the tube axis are obtained directly from the simulation. The transition process is shown in Fig. 3, which includes a series of snapshots of the atomic configurations of the molecules from the simulation. In the initial configuration starting at $T=500$ K [Fig. 3(a)], the molecules are in a liquid state with random orientations. During the cooling process, the molecules begin to align with the tube axis [Fig. 3(b)]. Further structural ordering is reached during the addi-
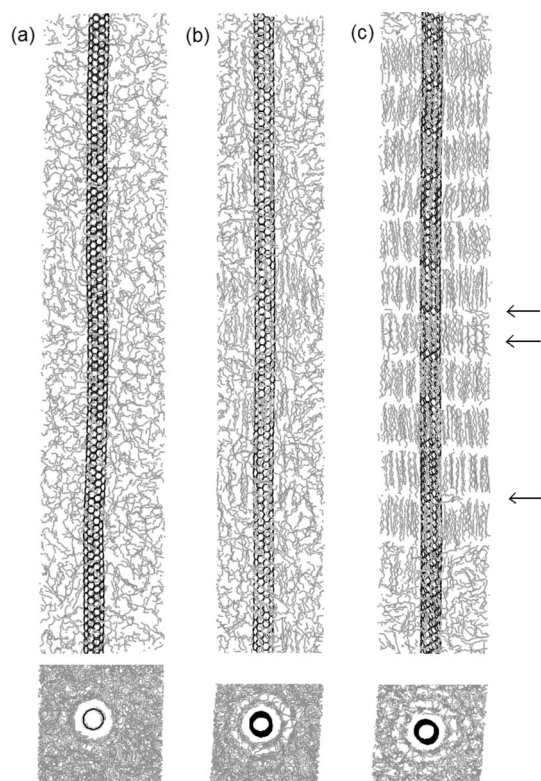
FIG. 3. Snapshots of atomic structures of decane CNT (5, 5) composite. (a) The starting configuration at $T=500$ K. (b) The configuration right after the cooling process at $T=300$ K. (c) The final configuration at the end of an additional 7 ns equilibrium run at $T=300$ K, after the cooling process. Decane molecules are colored in gray and the CNT in black. A few molecules trapped between the layers and a defect region in one of the layers are marked with arrows. Top views are shown at the bottom.

tional 7 ns run at $T=300$ K, as shown in Fig. 3(c). The ordered structures are formed in two ways: (1) strong molecule orientation alignments with the nanotube and (2) lamellar layer structures along Z, the tube axis direction. In Fig. 4, the molecule density profile shows a total of 11 decane molecule layers formed along the tube axis, with each layer about 10 Å in thickness (approximately the length of a straight decane molecule) and separated by ∼5 Å. Individual decane molecule is mostly in a straight configuration (or its dihedral angles in *trans* state) for the system shown in Fig. 3(c), which will be discussed in more details later. Near the unit cell boundary, there is no layer structures, as shown in Fig. 3(c). This is attributed to the constraints posted by the mismatch between the length of the simulation unit cell along the nanotube and that of the lamellar layers. This limitation is geometric in nature and a longer simulation up to 15 ns did not remove such region. Within each lamellar layer, the molecules are well aligned with the nanotube axis with a two-dimensional structure ordering in planes perpendicular to the tube axis [there is a few molecules trapped between the layers and there is a defect region at the edge of one of the layers, marked with arrows in Fig. 3(c)]. As an example, the snapshot of the atomic configuration of one of the layers (98 Å<Z<121 Å) is shown in Fig. 5 in top view. Nine
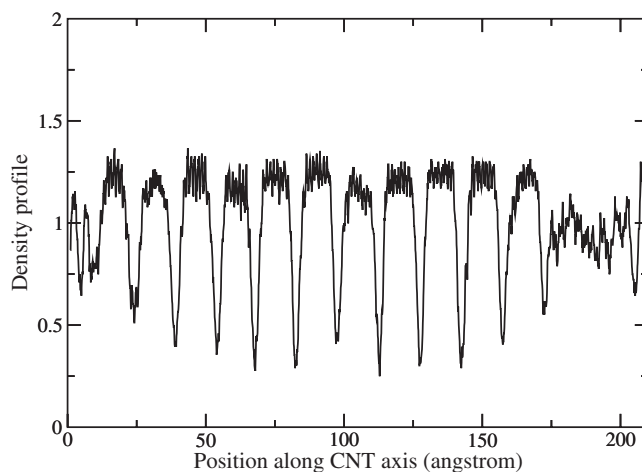

FIG. 4. The density profile (C atoms only) of decane molecules as a function of their position along the CNT axis for the configuration shown in Fig. 3(c). The unit for the density is arbitrary.

repeating unit cells are included and other layers have similar structures. The embedded CNT is shown in black bonds and the decane molecules are shown in gray bonds (only carbon atom shown). It can be seen that the molecule orientation is along the nanotube axis dominantly. More importantly, there is a two-dimensional translation ordering in the structure with the decane molecules in periodic arrays. In analogy to the crystalline structure of polyethylene (PE) molecules, a unit cell defined by two vectors $\vec{a}$ and $\vec{b}$ is marked in Fig. 5, with two decane molecules within the cell. The lengths of $|a|$ and $|b|$ are calculated as 4.67 ± 0.02 Å and 8.02 ± 0.03 Å, respectively, from direct geometry analysis on the positions of the center mass of all the molecules in the lamellar layers. The angle between $\vec{a}$ and $\vec{b}$ is calculated as $89.5°\pm7.5°$. The
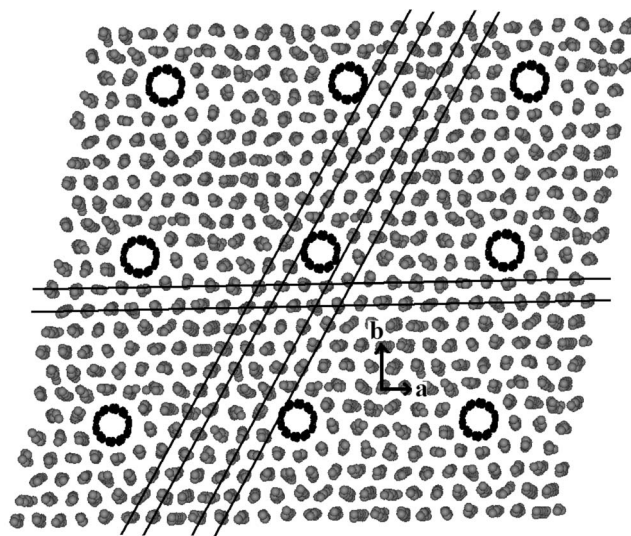

FIG. 5. Snapshot of atomic configurations of decane molecules in one of the lamellar layers shown in Fig. 3(c) (nine repeating unit cells shown). A unit cell with vectors $\vec{a}$ and $\vec{b}$ is shown. Some molecule arrays are marked with solid lines. Decane molecules are colored in gray and the CNT in black.
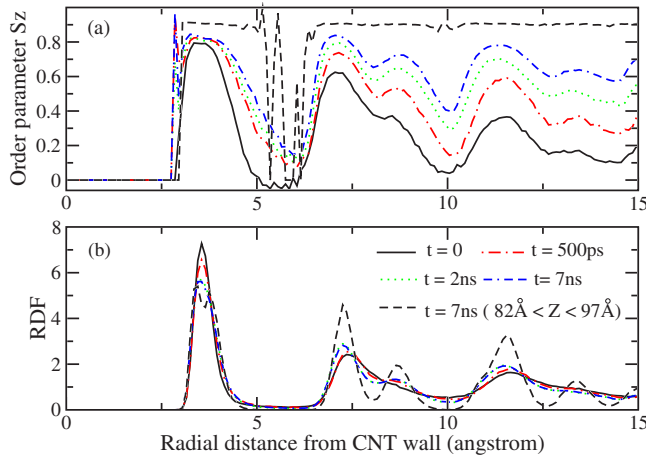
FIG. 6. (Color online) (a) The order parameter $S_z(r)$ at various of times during a 7 ns additional equilibrium run for the decane CNT (5, 5) composite at $T=300$ K. (b) $g(r)$ at various of times. The solid, dot-dashed, dotted, and dot-dash-dashed curves are for $t=0$, 500 ps, 2 ns, and 7 ns, respectively. The dashed curve is for the molecules in one of the lamellar layers at $t=7$ ns.

geometry of this unit cell is similar as in crystalline PE, where $|a|$ and $|b|$ are 4.94 and 7.41 Å, and the angle in between is 90°.[39] While in the crystalline structure the orientation of the backbone plane of a PE molecule along its long axis is restricted, such orientation has a broad distribution in the ordered structure formed around the nanotube. This suggests that the two-dimensional structure ordering is smectic phase in nature. The origin of the less perfect crystalline structure in the CNT composite is attributed to the fact that the CNT acts as a nucleation site in the phase transition. The decane molecules prefer planar configurations when adsorbed on the CNT surface, which would influence the orientations of the backbone planes of other molecules in further adsorption layers during the molecule packing process.

Evolutions of the ordering parameter $S_z(r)$ with time during the phase transition are shown in Fig. 6(a), obtained from the extended 7 ns equilibrium run at $T=300$ K. It can be seen that at $t=0$, the decane molecules in the first adsorption layer are already strongly aligned with the nanotube axis, and the strong alignments are extended to farther layers with time. This point is more evident from the $S_z(r)$ for the molecules in individual lamellar layer. An almost uniform $S_z(r) \rightarrow 1$ is shown in Fig. 6(a) (dashed line) for a sample layer (82 Å $<Z<$ 97 Å). Similarly, the evolution of $g(r)$ with time is shown in Fig. 6(b). At the initial time $t=0$, the oscillation feature in $g(r)$ with peaks at 3.5, 7.2, and 11.5 Å are similar, as shown in Fig. 1(a). With the evolvement of time, extra peaks at 8.7 and 13.3 Å emerge, due to the formation of the two-dimensional ordering for the molecules around the CNT as discussed above.

The process of the smectic phase transition in the decane CNT (5, 5) composite at molecular level is obtained directly from the MD simulations. Shown in Fig. 7 (color online) is a series of snapshots of the atomic configurations of decane molecules around the nanotube at $T=300$ K (during the extended 7 ns run). For illustration purpose only selected molecules are shown, and note that the molecule packing process
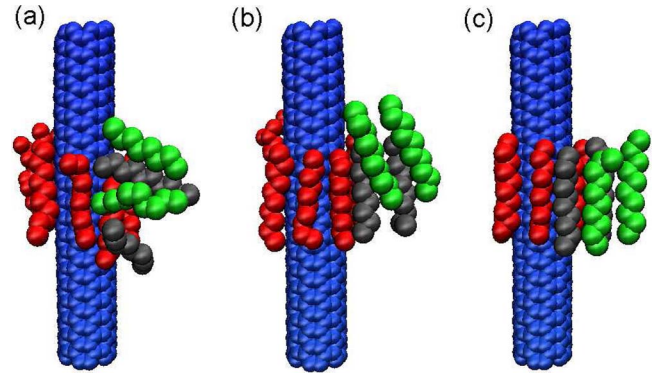

FIG. 7. (Color online) Snapshots of atomic configurations of CNT (5, 5) composite during the phase transition process at $T=300$ K, obtained from the additional 7 ns run after the cooling process. (a) $t=0$; (b) $t=0.2$ ns; (c) $t=0.3$ ns. Carbon atoms on CNT are colored in blue, molecules in first adsorption layer are marked in red, and molecules in further layers in gray and green (only selected molecules and a portion of the CNT are shown for clarification).

is local. At $t=0$, an adsorption layer (colored in red) at the CNT surface is already formed from the cooling process, while molecules at larger radial distance are in less ordered structures regarding their orientations and translational symmetry [Fig. 7(a)]. During the further simulation up to $t=0.2$ ns, these less ordered molecules (colored in grey) diffuse and reorient to form packed structures with the molecules already in the first adsorption layer [Fig. 7(b)]. Similar process is extended to the molecules (colored in green) at even larger radial distance with longer simulations up to $t=0.3$ ns [Fig. 7(c)]. This packing process agrees with a disk-shaped growth mechanism suggested in a recent experiment study on PE molecule crystallization in the presence of CNTs.[25]

In the structural phase shown in Figs. 3(c) and 5, the decane molecules have limited translational diffusions within the ordered lamellar layers, which is studied through mean square displacement (MSD) of molecules. Shown in Fig. 8 (solid line) is the MSD in planes perpendicular to the tube axis, for a chosen decane molecule, as a function of time (averaged over different starting time origins). The molecule is in one of the lamellar layers and also at the surface of the CNT. The limited values in the MSD suggest that the molecule is restricted to its local site (similar MSDs are obtained for other molecules within lamellar layers). In comparison, the MSD averaged over all the decane molecules outside the lamellar layer region[40] is also plotted in Fig. 8 (excluding the ones in the first adsorption layer, which have limited diffusions). The diffusion coefficient in the plane perpendicular to the CNT axis is estimated as $D_{xy} \sim 1.2 \times 10^{-5}$ cm²/s for molecules in the less ordered region, according to Einstein relation (fitted for $t>200$ ps),

$$D_{xy} = \lim_{t\to\infty} \frac{1}{4t} \langle [r(t+t_0) - r(t_0)]^2 \rangle. \quad (4)$$

This diffusion coefficient is comparable to that of molecule diffusions in a liquid state at room temperature. No molecule
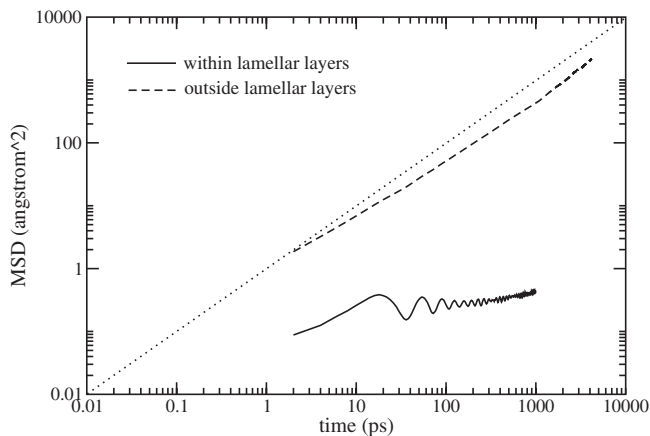
FIG. 8. The mean squared displacement (MSD) of decane molecules as a function of time (log-log scale) in the smectic phase of CNT (5, 5) composite at $T = 300$ K. Solid curve, for a molecule in the lamellar layers; dashed curve, for molecules outside the lamellar layers.

diffusion across the lamellar layers is observed after the layers are formed.

Different from the limited translational mobility discussed above, there are frequent molecule rotations along its own long axis, due to small energy barriers. Shown in Fig. 9(a) is the rotation angle φ of the backbone plane of a decane molecule (which is at the CNT surface and in one of the lamellar layers) around its long axis as a function of time. Free energy profile $f(\varphi)$ can be obtained from the distribution function $P(\varphi)$, according to Boltzmann distribution,

$$P(\varphi) = P_0 e^{-f(\varphi)/k_B T}, \qquad (5)$$

where P_0 is a constant. The corresponding $f(\varphi)$ for the molecule rotation shown in Fig. 9(a) is plotted in Fig. 9(b). The two φ's at the minimum of $f(\varphi)$ is shown at $\varphi_1 = 35°$ and
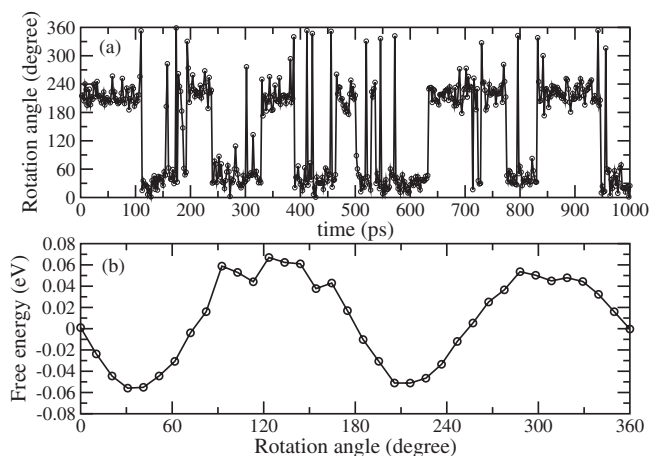

FIG. 9. (a) The rotation angle ϕ of a decane molecule (in one of the lamellar layers) along its own long axis as a function of time in the CNT (5, 5) composite at $T = 300$ K with the smectic phase [see Fig. 3(c)]. (b) Free energy $f(\phi)$ for the molecule rotation motion in (a) as a function of rotation angles, according to Eq. (5).

$\varphi_2 = 215°$, with a relation $\varphi_2 - \varphi_1 = 180°$. The origin of such relation is due to the fact that the two configurations at φ_1 and φ_2 are energetically equivalent by flipping the backbone plane of the molecule along its own long axis. The energy barrier that separated the two configurations is estimated as $E_v \sim 0.11$ eV $\approx 4.3 k_B T$ ($T = 300$ K). Free energy obtained in this way has less accuracy at the barrier heights than at the bottoms due to less statistical data accumulated at the higher energies. According to a diffusion model for polymer molecule rotation, the averaged flipping frequency can be expressed as follows:[41]

$$\langle \omega \rangle = \sqrt{\frac{2 k_B T}{\pi I}} e^{-E_v/k_B T}, \qquad (6)$$

where the molecular moment of inertia $I = \int m x^2 dx$ ($= \Sigma_i m_i x_i^2$ in case here, where i is the label for atoms). The prefactor $\omega_0 = \sqrt{2 k_B T / \pi I}$ depends on the geometry of the molecule. Taking the geometric fact of a decane molecule with bond length of 1.52 Å and bending angle of 112.8°, ω_0 is estimated as 2.5×10^{12} s^{-1}. Thus $\langle \omega \rangle$ is estimated as $\sim 3.4 \times 10^{10}$ s^{-1} at $T = 300$ K, according to Eq. (6) with $E_v \sim 0.11$ eV. The averaged flipping period is thus estimated as $\bar{T} = 2\pi/\langle \omega \rangle \sim 100$ ps, which is in the same order of magnitude of the duration times around φ_1 or φ_2 shown in Fig. 9(a). The value of $E_v \sim 0.11$ eV is rather at the upper limit for the rotation barriers. More detailed analysis shows an averaged $\bar{E}_v \sim 2.0 k_B T$ and $\sim 1.5 k_B T$ ($T = 300$ K) for molecules in the first and second adsorption layers, respectively. The barrier for molecules at farer radial distances from CNT wall is even smaller with $\bar{E}_v \sim 1.0 k_B T$ ($T = 300$ K). The higher $\bar{E}_v$ at the CNT surface can be attributed to the stronger attractive interfacial interactions for the molecules with the nanotube than with the polymer matrix medium and $\bar{E}_v$ is expected to increase linearly with the molecule length for a longer molecule in a similar structure phase.

To investigate the influence of atomic structures of CNT lattices on molecule structure phases, a composite consisting of 800 decane molecules and a continuous 210 Å long zigzag CNT (10, 0) are prepared similarly with the procedure described above. The RDF $g(r)$ and order parameter $S_z(r)$ are plotted in Fig. 10 for various temperatures. The oscillation features in $g(r)$ and $S_z(r)$ and the enhancement in the magnitudes of adsorption peaks with decreasing T are similar as in the composite consisting of an armchaired CNT (5, 5). There are two differences though. One is that there is no peak around $r = 8.4$ Å adjoined to the second adsorption peak in the CNT (10, 0) composite. Appearance of such peak has been related to the two-dimensional structure ordering in the smectic phase observed in the CNT (5, 5) composite. The other difference is that while there is significant molecule alignment along the nanotube axis in the CNT (10, 0) composite, such alignment is less in magnitude compared with the one embedded with CNT (5, 5), especially for distributions beyond the first adsorption layer, when comparing $S_z(r)$'s [Fig. 1(b) and Fig. 10(b)].

A snapshot of the atomic configuration of the CNT (10, 0) composite at $T = 300$ K is shown in Fig. 11, which is ob-
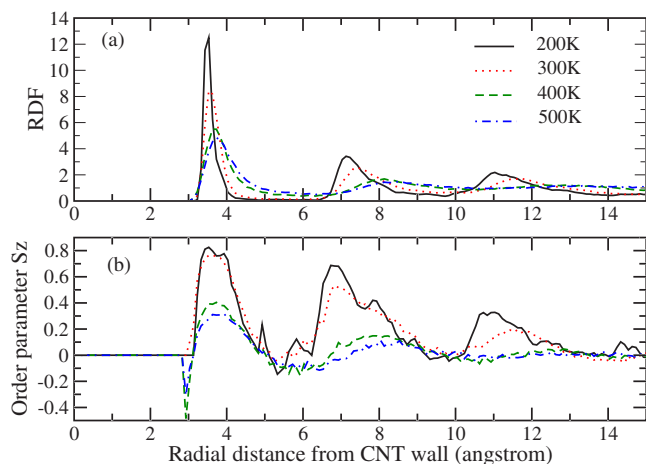
FIG. 10. (Color online) (a) The radial distribution function (RDF) for decane molecules in CNT (10, 0) composite. (b) The orientation order parameter $S_z(r)$. Solid, dotted, dashed, and dot-dashed lines are for $T=200$, 300, 400, and 500 K, respectively, in both (a) and (b).

tained from an extended 6.4 ns equilibrium MD simulation right after the system is cooled down from high temperatures. No lamellar layers or two-dimensional translation ordering are observed, which is different from the uniform molecule alignment around CNT (5, 5). We attribute the origin of the differences to influences of nanotube chirality on molecule conformations. As discussed above, a CNT acts as a nucleation site in the decane molecule packing and crystallization process and the atomic structure of the embedded CNT is expected to affect such process. Previous MD studies show that polymer molecule conformations at a nanotube interface depends on the radius and chirality of the tube,[18] due to the combined contributions to the adsorption energy from the molecular coiling energy E_c around the tubular CNT and the interfacial interaction energy E_l with the nanotube, which depends on the registry between a polymer molecule and the CNT lattice. While $E_c = k_c \sin^4 \theta / R^2$ (k_c, θ, and R is bending constant, coiling or wrapping angle, and coiling radius of a molecule, respectively)[42] prefers small wrapping angles for molecules around a nanotube, E_l favors conformations commensurate with the substrate nanotube lattice. The commensurate configuration for a decane molecule would require wrapping angle $\theta=0°$ or 60° around an armchaired CNT, while require $\theta=30°$ or 90° on a zigzag tube. The total potential energy of a molecule adsorbed on a nanotube can be expressed as $E = E_c + E_l = k_c \sin^4 \theta / R^2 + \delta E_l(\theta) + E_0$, where

FIG. 11. Snapshot of the atomic configuration of the decane CNT (10, 0) composite at the end of an additional 6.4 ns equilibrium run at $T=300$ K (see text for details). Decane molecules are colored in gray and the CNT in black. Left, side view; right, top view.
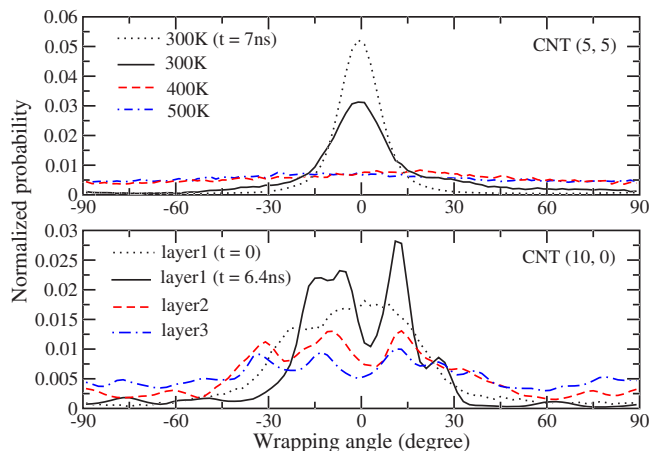

FIG. 12. (Color online) Normalized probability function $P(\theta)$ of decane molecules as a function of wrapping angles [see inset of Fig. 1(a) and text for detail]. (a) CNT (5, 5) composite: for molecules in the first adsorption layer. The solid, dashed, and dot-dashed curves are for $T=300$, 400, and 500 K during the cooling process, respectively. The dotted curve is for $T=300$ K after an additional 7 ns equilibrium run. (b) CNT (10, 0) composite: for molecules in the first, second, and third adsorption layers at $T=300$ K. The dotted curve is for molecules in first adsorption layer at $t=0$ right after the cooling process. The solid, dashed, and dot-dashed curves are for molecules in the first, second, and third adsorption layers after an additional 6.4 ns equilibrium run, respectively.

E_0 is a constant for adsorption energy and the $\delta E_l(\theta)$ is a correction term for E_0 from the registry effect between the molecule and the CNT lattice. Previous study has shown that PE molecules prefer 0° wrapping angle dominantly on a small radius armchaired CNT (5, 5) surface, which conformation is energetic favorable from both the coiling energy and interactions with the CNT lattice contributions. However, on a similar radius zigzag CNT (10, 0), PE molecules prefer rather different wrapping angles away from 0°, as E_l is not favorable at such angle on the zigzag tube.[18] Though the decane molecules we study here is shorter than the PE molecule with 100 monomers in the previous study, it is expected that the molecule conformation behavior would be similar.

Shown in Fig. 12 is the normalized probability function $P(\theta)$ for a local wrapping angle θ between the vector (projected to planes parallel to the nanotube surface) connecting the two ends of a three-segment subchain on a decane molecule and the nanotube axis [see Fig. 1(a) inset for illustration]. As discussed above, a dominated peak at $\theta=0°$ appears around CNT (5, 5) when T is decreased from 500 to 300 K during the cooling process, as seen in Fig. 12(a) (only contribution from the molecules in the first adsorption layer included). The peak at 0° is further enhanced during the extended 7 ns run at $T=300$ K. In comparison, a broader distribution is seen for molecules around CNT (10, 0), as shown in Fig. 12(b). During the extended 6.4 ns equilibrium simulation at $T=300$ K, two distinct peaks around $\theta \sim 12°$, [$-13°, -5°$], and a small peak at 25° can be seen for the molecules in the first adsorption layer. The value of $P(\theta)$ for the first layer is significantly decayed for $|\theta|>30°$. Beyond
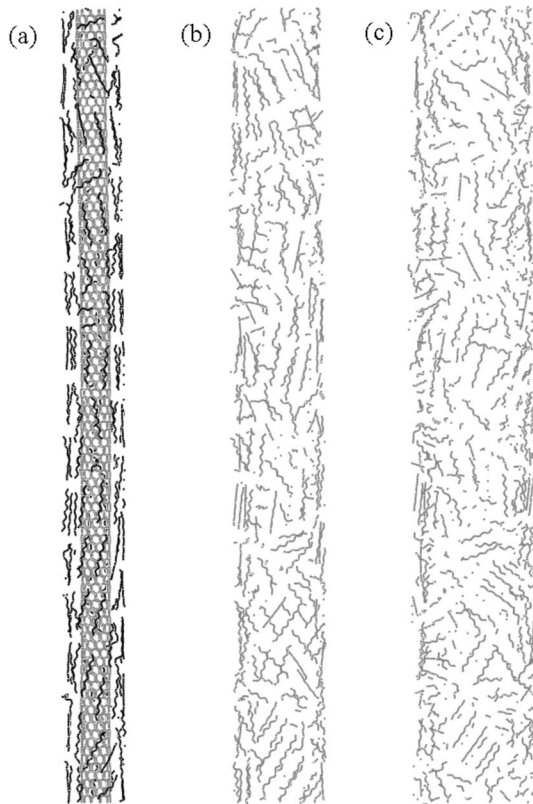
FIG. 13. Snapshots of the atomic configurations of decane molecules in the adsorption layers around CNT (10, 0) at the end of the 6.4 ns additional run at $T=300$ K. (a) First adsorption layer; (b) second adsorption layer; (c) third adsorption layer.
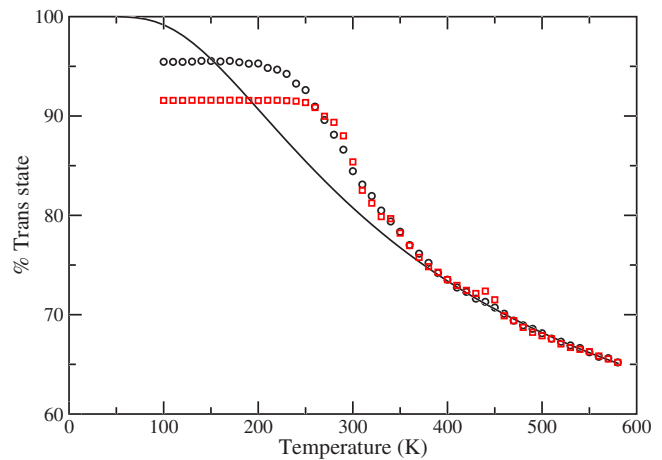

FIG. 14. (Color online) The percentage of decane molecule dihedral angles in *trans* states as a function of temperature. Circle and square symbols are for CNT (5, 5) and (10, 0) composites, respectively. Solid curve is a theoretical fitting according to Boltzmann distribution at high T's.

the angle of 30°, the molecule coiling energy $E_c = k_c \sin^4 \theta / R^2$ would be larger than 0.3 meV per monomer, considering $k_c = L_p k_B T$ with $L_p \sim 10$ Å at $T=300$ K[43], decane molecule length $L \sim 10$ Å, and $R \approx (3.5+3.9)$ Å for molecules in the first adsorption layer around the CNT (10, 0). The energy gains $|\Delta E_l|$ (the maximum of $|\delta E_l(\theta)| \approx 0.3$ meV per monomer) for a decane molecule commensurate with the nanotube lattice than incommensurate configurations would be overwritten by the increased coiling energies for $|\theta| > 30°$. This consideration suggests that k_c or ΔE_l can serve as a tunable parameter for $P(\theta)$, and a stiff polymer or a small $|\Delta E_l|$ would induce narrow wrapping angle distributions.

The $P(\theta)$ for molecules in the second and third adsorption layers in CNT (10, 0) composite is also shown in Fig. 12(b). The peaks in these further layers follow that from the first adsorption layer. This is attributed to the fact that the packing of the decane molecules is in layer by layer fashion, starting from the nanotube nucleation site. There are emerging peaks at large angles in $P(\theta)$ for the second and third adsorption layers, as the energy cost of molecule coiling is decreased with increasing of radius. The snapshot of the configurations of the decane molecules in the first three adsorption layers is shown in Fig. 13 (from the configuration at the end of the 6.4 ns equilibrium run at $T=300$ K). It can be seen that the molecules align with the tube with tilted wrapping angles in

domains in all the three layers. Such domain pattern is shown to be entropy driven.[18] While a uniform non-0° wrapping angle would have the molecules in a twisted configuration around the CNT (10, 0), the diverse domains make the molecule structural phase more complicated. Also note that the distributions of $P(\theta)$ in the CNT (10, 0) composite would depend not only on potential energies but also on entropies from domain distributions. The dynamics for the domains regarding their distributions and interactions would need further studies.

As we mentioned previously, an individual molecule undergoes a conformation transition from a coiled configuration to an extended one with its dihedral angle changing from *gauche* states to *trans* state when T decreases. Such transition is present in both the CNT (5, 5) and (10, 0) composites. The percentage of *trans* state $\langle X_t \rangle$ for dihedral angle ϕ in decane molecules as a function of T is shown in Fig. 14 for both composites, where ϕ is defined as in *trans* state if $-60° < \phi < 60°$ or in *gauche* states if otherwise. From Fig. 14, it can be seen that $\langle X_t \rangle$ rises exponentially with decreasing T until the transformation from *gauche* to *trans* state begin to freeze at low T_s. The energy difference between *trans* and *gauche* states, $\Delta E_\phi / k_B = 504$ K is obtained through the fitting of the distribution at high T's according to Boltzmann distribution $\langle X_t \rangle / \langle X_g \rangle \propto e^{\Delta E_\phi / k_B T}$, where the percentage of *gauche* states is related to that of *trans* state as $\langle X_g \rangle = 1 - \langle X_t \rangle$. In comparison, the stationary $\Delta E_\phi^0 / k_B = 530$ K is calculated according to the force field used here for the dihedral angles, which is higher than the value obtained from the simulation. This difference can be attributed to the exclude volume effects included in the simulations, which would prevent some sequence *gauche-gauche* conformations in the molecules.[44] The decane molecules in the CNT (5, 5) have higher $\langle X_t \rangle$ at low T's as compared to that in CNT (10, 0), which can be attributed to the stronger molecule alignment with the embedded nanotubes in the former case.

One of the other factors that would influence the structure

phase of polymer molecules is the strength and nature of the interfacial interactions with the embedded nanotubes. Based on an elastic model for a polymer molecule adsorbed on a surface, which considers the balance between the molecule adsorption energy and confinement entropy at the surface, the thickness of the molecule can be expressed as follows:[45]

$$D = \frac{2bk_BT}{\epsilon}, \tag{7}$$

where b is one bond distance of the molecule from the surface and ϵ is the adsorption energy per monomer. To have a molecule adsorbed on a surface in planar configurations with $D \sim b$, the adsorption energy needs to satisfy $\epsilon > 2k_BT \sim 50$ meV ($T=300$ K) per monomer according to Eq. (7). This is the case for decane molecules studied here, where the vdw attractive interactions provide a $\epsilon \sim 80$ meV per monomer between the molecules and a graphite and the adsorption energy would be enhanced around a nanotube surface due to a curvature effect. A recent continuum field theory also shows an adsorption-desorption transition for a polymer molecule around a tubular surface with a critical ϵ^* for the interfacial adsorption strength, and a molecule would adsorb on the surface with a planar configuration when $\epsilon > \epsilon^*$.[46]

In a general sense, both polymer adsorption on and depletion from CNTs can happen, depending on the nature of the interfacial interactions, which are shown to be complicated for polymers with complex structures and compositions.[48–51] The influence of a repulsive surface is also studied through a model interaction. A usual vdw interaction potential in the truncated 12-6 LJ form is expressed as follows:

$$V_{ij}(r) = 4\epsilon \left[\left(\frac{\sigma}{r} \right)^{12} - \left(\frac{\sigma}{r} \right)^6 \right], \tag{8}$$

where the first term is for a repulsion interaction at near distances, and the second term is for an attractive interaction at large distances. To model a repulsive surface, a potential of $V_{ij}^n = 4\epsilon(\sigma/r)^{12}$ is used for interactions between CNTs and molecules.[47] A composite consisting of 800 decane molecules and a continuous CNT (5, 5) with length of 210 Å was prepared with the similar procedure described above. The $g(r)$ of the system is shown in Fig. 15(a) for $T=300$, 400, and 500 K. The function $g(r)$ has flat distributions and there is no molecule adsorption layer, due to the lack of attractive interactions with the nanotube. Such density profile feature is similar as the depletion layers on a repulsive polymer solid surface.[52] The configurations of the decane molecules at the repulsive surface are also very different from the ones with the full LJ potential. Instead of wrapping around the nanotubes, the molecules prefer tilted orientations away from the nanotube surface as illustrated in the inset of Fig. 15(b). Shown in Fig. 15(b) is the normalized probability function $P(\beta)$ as a function of the tilting angle β between the vector (projected to planes perpendicular to the nanotube surface) connecting the two ends of a three-segment subchain on a decane molecule and the nanotube axis. It can be seen that when T is lowered to 300 K, the molecules prefer large $\beta > 50°$. A snapshot of the equilibrium configuration of the system at $T=300$ K is shown in Fig. 16, in which some
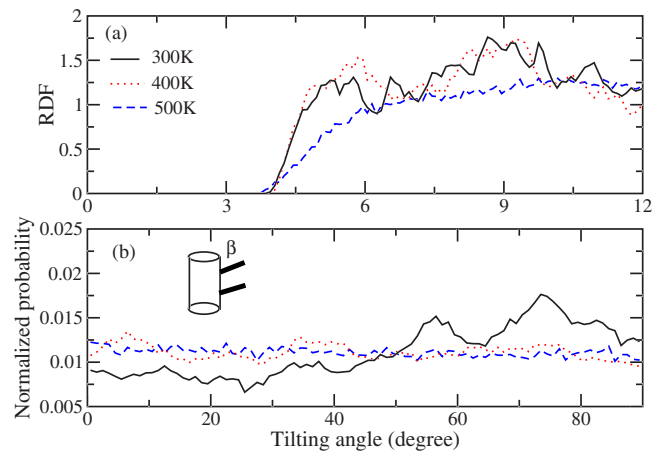

FIG. 15. (Color online) (a) The radial distribution function (RDF) for a decane CNT (5, 5) composite with a model repulsive interfacial interaction with the embedded nanotubes. (b) The normalized probability function $P(\beta)$ as a function of molecule tilting angle β from CNTs. Inset: illustration of molecules (black straps) with tilting angle β away from a CNT surface. Solid, dotted, and dashed curves are for $T=300$, 400, and 500 K, respectively, in both (a) and (b).

decane molecules can be seen with orientations in a nearly perpendicular direction to the nanotube surface, in a brush-like configuration. Further studies would be needed to gain more understandings about the interfacial interaction effects on the polymer structural phases and their transitions in a nanotube composite.

The crystallization of PE molecules in CNT composites has been studied in several recent experiments, where lamellar layer structures of molecules in alignment with embedded CNTs have been observed[24] and a disk-shaped growth mechanism in the molecule crystallization process has also been suggested,[25] similar as shown in the simulations. Though nanotube composites with short decane molecules are investigated in this study, similar phase transition process
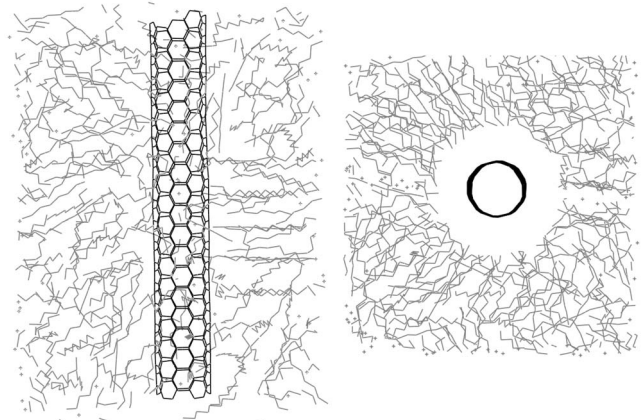

FIG. 16. Snapshot of the atomic configuration of a decane CNT (5, 5) composite with a model repulsive interfacial interaction, at $T=300$ K. Only portion of the system is shown. Left, side view; right, top view.

for longer chained polymer composites is expected, due to the fact that the embedded CNTs act as nucleation sites. The conformation of a short or long molecule at a nanotube surface is affected similarly by the geometric coiling energy and the CNT chirality dependent interfacial vdw interactions, which plays a determined role in the molecule packing process in further layers around the nanotube. However, for a long polymer molecule, more complicated conformation arrangements can exist such as the self-folding of chains as observed in experiment.[24] Highly ordered molecule structures and enhanced crystallization have also been observed in other type of polymer CNT composites or hybrid systems, such as with conjugated polymers[12,13,16,19] or even DNA molecules.[8,17] Detailed molecule structures and interfacial interactions are expected to affect structure phases and their transitions.

In summary, the structural phase transition and related properties of polymer molecules in various CNT composites are studied through MD simulations. Decane molecules are found to undergo a smectic transition around an armchaired CNT (5, 5), forming lamellar layers with two-dimensional structure ordering in each layer. The molecule packing and crystallization process is in layer by layer fashion with the embedded CNT as a nucleation site. While the translational diffusions of decane molecules in the lamellar layers are restricted, the rotations of molecules along their own long axis are rather free with small energy barriers $\bar{E}_v \sim 1-2k_BT$ ($T=300$ K). Neither lamellar layer structures nor two-dimensional ordering of decane molecules are formed in a similar radius but different chirality zigzag CNT (10, 0) composite, due to the diverse conformation domains with non-0° wrapping angles, which resulted from the molecule interfacial interactions with the nanotube lattice. Studies also show that the nature and the strength of the interfacial interactions play crucial roles in structural phases of molecules in a nanotube composite. This study is expected to be important not only for the fundamental understanding of structural phases and their transitions in composite materials but also for the applications of CNT based composites.

*cwei@mail.arc.nasa.gov

[1] For detailed review, see *Carbon Nanotubes: Synthesis, Structure, Properties, and Applications*, edited by M. S. Dresselhaus, G. Dresselhaus, and P. Avouris (Springer, New York, 2000).

[2] P. M. Ajayan, L. S. Schadler, C. Giannaris, and A. Rubio, Adv. Mater. (Weinheim, Ger.) **12**, 750 (2000).

[3] D. Qian, E. C. Dickey, R. Andrews, and T. Rantell, Appl. Phys. Lett. **76**, 2868 (2000).

[4] M. Cadek, J. N. Coleman, K. P. Ryan, V. Nicolosi, G. Bister, A. Fonseca, J. B. Nagy, K. Szostak, F. Bguin, and W. J. Blau, Nano Lett. **4**, 353 (2004).

[5] B. Kim, J. Lee, and I. Yu, J. Appl. Phys. **94**, 6724 (2003).

[6] R. Ramasubramanjam, J. Chen, and H. Liu, Appl. Phys. Lett. **83**, 2928 (2003).

[7] B. E. Kilbride, J. N. Coleman, J. Fraysse, P. Fournet, M. Cadek, A. Drury, S. Hutzler, S. Roth, and W. J. Blau, J. Appl. Phys. **92**, 4024 (2002).

[8] M. Zheng, A. Jagota, M. S. Strano, A. P. Santos, P. Barone, S. G. Chou, B. A. Diner, M. S. Dresselhaus, R. S. Mclean, G. B. Onoa, G. G. Samsonidze, E. D. Semke, M. Usrey, and D. J. Walls, Science **302**, 1545 (2003).

[9] K. Besteman, J.-O. Lee, F. G. M. Wiertz, H. A. Heering, and C. Dekker, Nano Lett. **3**, 727 (2003).

[10] K. Bradley, M. Briman, A. Star, and G. Gruner, Nano Lett. **4**, 253 (2004).

[11] M. J. Moghaddam, S. Taylar, M. Gao, S. Huang, L. Dai, and M. J. McCall, Nano Lett. **4**, 89 (2004).

[12] R. Czerw, Z. Guo, P. M. Ajayan, Y.-P. Sun, and D. L. Carroll, Nano Lett. **1**, 423 (2001).

[13] B. McCarthy, J. N. Coleman, R. Czerw, A. B. Dalton, M. Panhuis, A. Maiti, A. Drury, P. Bernier, J. B. Nagy, B. Lahr, H. J. Byrne, D. L. Carroll, and W. J. Blau, J. Phys. Chem. B **106**, 2210 (2002).

[14] H. Ago, R. Azumi, S. Ohshima, Y. Zhang, H. Kataura, and M. Yumura, Chem. Phys. Lett. **383**, 469 (2004).

[15] B. Philip, J. Xie, J. K. Abraham, and V. K. Varadan, Smart Mater. Struct. **13**, 105 (2004).

[16] R. G. S. Goh, N. Motta, J. M. Bell, and E. R. Waclawik, Appl. Phys. Lett. **88**, 053101 (2006).

[17] D. A. Heller, E. S. Jeng, T.-K. Yeung, B. M. Martinez, A. E. Moll, J. B. Gastala, and M. S. Strano, Science **311**, 508 (2006).

[18] C. Wei, Nano Lett. **6**, 1627 (2006).

[19] M. Cadek, J. N. Coleman, V. Barron, K. Hedicke, and W. J. Blau, Appl. Phys. Lett. **81**, 5123 (2002).

[20] B. P. Grady, F. Pompeo, R. L. Shambaugh, and D. Resasco, J. Phys. Chem. B **106**, 5852 (2002).

[21] A. R. Bhattacharyya, T. V. Sreekumar, T. Liu, S. Kumar, L. M. Erison, R. H. Hauge, and R. E. Smalley, Polymer **44**, 2373 (2003).

[22] L. Valentini, J. Biagiotti, and M. A. Lopez-Manchardo, Polym. Eng. Sci. **44**, 303 (2004).

[23] P. Miaudet, S. Badaire, M. Maugey, A. Derre, V. Pichot, P. Launois, P. Poulin, and C. Zakri, Nano Lett. **5**, 2212 (2005).

[24] L. Li, C. Y. Li, and C. Ni, J. Am. Chem. Soc. **128**, 1692 (2006).

[25] R. Haggenmueller, J. E. Fischer, and K. I. Winey, Macromolecules **39**, 2964 (2006).

[26] J. N. Coleman, W. J. Blau, A. B. Dalton, E. Muoz, S. Collins, B. G. Kim, J. Razal, M. Selvidge, G. Vieiro, and R. H. Baughman, Appl. Phys. Lett. **82**, 1682 (2003).

[27] J. N. Coleman, M. Cadek, K. P. Ryan, A. Fonseca, J. B. Nagy, W. J. Blau, and M. S. Ferreira, Polymer **47**, 8556 (2006).

[28] C. Wei, Appl. Phys. Lett. **88**, 093108 (2006).

[29] DLPOLY code is used and is obtained from Darebury Laboratory, UK.

[30] W. D. Cornell, P. Cieplak, C. I. Bayly, I. R. Gould, K. M. Merz, D. M. Ferguson, D. C. Spellmeyer, T. Fox, J. W. Caldwell, and P. A. Kollman, J. Am. Chem. Soc. **117**, 5179 (1995).

[31] J. Tersoff, Phys. Rev. B **37**, 6991 (1988); D. W. Brenner, *ibid.* **42**, 9458 (1990).

[32] C. Wei, D. Srivastava, and K. Cho, Nano Lett. **2**, 647 (2002).

[33] The radial distance r is defined as the distance between the center of mass of a subchain with four segments on a same molecule and the nanotube surface along its radial direction.

[34] C. Wei, D. Srivastava, and K. Cho, Nano Lett. **4**, 1949 (2004).

[35] I. Bitsanis and G. Hadziioannou, J. Chem. Phys. **92**, 3827 (1989).

[36] S. K. Kumar, M. Vacatello, and D. Y. Yoon, Macromolecules **23**, 2189 (1990).

[37] D. Rigby and R.-J. Roe, J. Chem. Phys. **89**, 5280 (1988).

[38] P. G. deGennes, Mol. Cryst. Liq. Cryst. **12**, 193 (1971).

[39] F. W. Billmeyer, Jr., *Textbook of Polymer Science* (Wiley, New York, 1984), Chap. 10.

[40] A molecule is considered to be outside the lamellar layer region if the position of its center of mass along the nanotube axis Z satisfies $Z < 10$ Å or $Z > 175$ Å, as shown in Fig. 4.

[41] D. E. O'Reilly and T. Tsang, J. Chem. Phys. **46**, 1291 (1967).

[42] M. Doi and S. F. Edwards, *The Theory of Polymer Dynamics* (Clarendon, Oxford, 1986), p. 317.

[43] P. J. Flory, *Statistical Mechanics of Chain Molecules* (Inter-science, New York, 1969).

[44] D. Brown and J. H. R. Clarke, Macromolecules **24**, 2075 (1991).

[45] K. A. Den and S. Bromberg, *Molecular Driving Forces: Statistical Thermodynamics in Chemistry and Biology* (Garland Science, New York, 2002), p. 637.

[46] E. Eisenriegler, A. Hanke, and S. Dietrich, Phys. Rev. E **54**, 1134 (1996).

[47] $\sigma = 3.65$ Å and $\epsilon = 0.461$ kJ/mol, with cutoff distance of 9.875 Å is used.

[48] K. Liao and S. Li, Appl. Phys. Lett. **79**, 4225 (2001).

[49] D. W. Steuerman, A. Star, R. Narizzano, H. Choi, R. S. Ries, C. Nicolini, J. F. Stoddart, and J. R. Heath, J. Phys. Chem. B **106**, 3124 (2002).

[50] M. Yang, V. Koutso, and M. Zaiser, J. Phys. Chem. B **109**, 10009 (2005).

[51] I. Vasiliev and S. A. Curran, Phys. Rev. B **73**, 165420 (2006).

[52] P. G. de Gennes, Adv. Colloid Interface Sci. **27**, 189 (1987).